Nickel coordination compounds of the cyanamido squarate ligand. The crystal structures of the 2,4-bis(cyanamido)cyclobutane-1,3-dione dianion (2,4-NCNsq^{2-}) and of three polymers with general formula $[Ni(Him)_x(H_2O)_{4-x}(2,4\text{-}NCNsq)\cdot yH_2O]_n$ ($x = 2$–4; $y = 1$–3; Him = imidazole)

Olivier Cortadellas [a], Anne Marie Galibert [a,*], Brigitte Soula [a], Bruno Donnadieu [b], Paul-Louis Fabre [a]

[a] *Laboratoire de Chimie Inorganique, EA 807, Université Paul Sabatier, Bat. II R1, 118 Route de Narbonne, 31062 Toulouse Cedex 04, France*
[b] *Laboratoire de Chimie de Coordination, UPR CNRS 8241, 205 Route de Narbonne, 31077 Toulouse Cedex 04, France*

Abstract

Disodium and ditetraphenylphosphonium salts of 2,4-bis(cyanamido)cyclobutane-1,3-dione, $Na_2(2,4\text{-}NCNsq)\cdot 2H_2O$ (**1**) and $(Ph_4P)_2(2,4\text{-}NCNsq)\cdot 4H_2O$ (**2**) have been synthesized and used to prepare three nickel(II) complexes: $[Ni(Him)_4(2,4\text{-}NCNsq)\cdot 2H_2O]_n$ (**3**), $[Ni(Him)_3(H_2O)(2,4\text{-}NCNsq)\cdot H_2O]_n$ (**4**) and $[Ni(Him)_2(H_2O)_2(2,4\text{-}NCNsq)\cdot 3H_2O]_n$ (**5**). Compounds **1**–**5** have been synthesized and characterized by electronic absorption and IR spectroscopies and by electrochemical studies. The structures of the salt **2** and of the complexes **3**–**5** have been determined by X-ray crystallography. The dianion of **2** presents a centro-symmetric square planar structure with two NCN functions deviated from the ring plane by an angle of 20.6°. Complexes **3**–**5** are polynuclear nickel(II) compounds containing 2,4-NCNsq^{2-} bridging ligands. These ligands are coordinated by the nitrile nitrogen atoms of the cyanamido functions and lie in *cis* (complex **4**) or *trans* (complexes **3** and **5**) positions in the coordination sphere of the nickel(II). The magnetic properties of the three complexes have been investigated in the 2–300 K temperature range ($\mu_{eff} = 2.79$–$3.34\ \mu_B$ for **3**, 2.76–3.25 μ_B for **4** and 3.14–3.46 μ_B for **5**). Their redox properties are discussed and compared to those of the free 2,4-NCNsq^{2-} dianion.

Keywords: Pseudo-oxocarbons; X-ray diffraction; Polynuclear nickel(II) complexes; Cyanamido squarate complexes

1. Introduction

Pseudo-oxocarbon compounds derived from the squarate dianion are characterized by extensive π electrons delocalization, interesting redox behaviour and, for some of them, strong colours and intrinsic electrical conductivity [1–5].

In the course of our studies on this class of compounds [6–10], we have focused our attention on cyanamido squarate derivatives as the 3,4-bis(cyanamido)cyclobutane-1,2-dione dianion (3,4-NCNsq^{2-}) and the 2,4-bis(cyanamido)cyclobutane-1,3-dione dianion (2,4-NCNsq^{2-}).

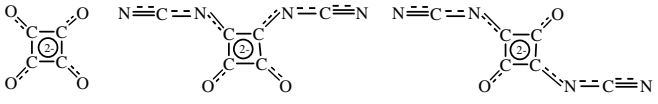

squarate dianion (sq^{2-}) 3,4-NCNsq^{2-} 2,4-NCNsq^{2-}

An analogy of the 2,4-NCNsq^{2-} dianion with the 1,4-dicyanamidobenzene dianion (dicyd^{2-}), the reduced form

* Corresponding author. Tel.: +33 561556119; fax: +33 561556118.
E-mail address: galibert@chimie.ups-tlse.fr (A.M. Galibert).

doi:10.1016/j.ica.2005.07.048

of DCNQI (dicyanoquinonediimine) may be proposed [11,12] because they show the same delocalized *trans* structure.

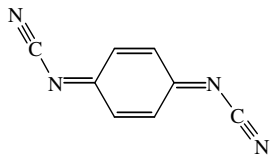

DCNQI

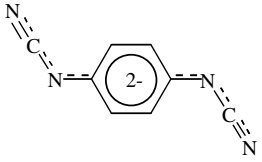

$dicyd^{2-}$

The well known interest in the DCNQI derivatives has raised since the discovery of radical anion copper salts presenting an increased conductivity as temperature is reduced. They have been considered as new organic metal systems [13–18].

The coordination chemistry of the cyanamido squarate dianions is expected to be as potentially rich as that of the phenylcyanamide ligands [19] and may lead to new complexes exhibiting magnetic exchange between metal ions [20], to molecular materials characterized by electron transport chains [18], or to electrochromic materials [21].

We have previously reported on copper(I), copper(II) [8], nickel(II) [9] and Pd(II) [10] complexes with the 3,4-$NCNsq^{2-}$ ligand. In these complexes, the dianion occurs as a monodentate or bis-monodentate ligand, bonding via either the nitrile function or the amido nitrogen atom. In the case of nickel(II) chains, it was shown to propagate weak antiferromagnetic interactions between the metal centres.

In the present paper, we report on the characterization of the 2,4-$NCNsq^{2-}$ dianion and on the synthesis and characterization of its first transition metal complexes, three polynuclear nickel(II) complexes: $[Ni(Him)_4(2,4\text{-}NCNsq)\cdot 2H_2O]_n$ (**3**), $[Ni(Him)_3(H_2O)(2,4\text{-}NCNsq)\cdot H_2O]_n$ (**4**) and $[Ni(Him)_2(H_2O)_2(2,4\text{-}NCNsq)\cdot 3H_2O]_n$ (**5**).

2. Experimental

2.1. General

All solvents and chemicals were reagent grade or better and used as received unless otherwise noted. Squaric acid, cyanamide and dien were purchased from Acros. The 2,4-dimethylaminocyclobutene diolate (2,4-$N(CH_3)_2sq$) was obtained according to Neuse et al. [22] by reaction of squaric acid with dimethylamine.

The complexes were isolated as air-stable crystals. UV–visible spectra have been performed in dmf solution on a Cary 1E spectrophotometer. IR spectra were recorded in the solid state in KBr pellets or in dmf solution using a 1760-X Perkin–Elmer Infrared Fourier Transform spectrometer. In the 2–300 K temperature range, magnetic susceptibility measurements were collected for powdered samples using a SQUID-based sample magnetometer on a QUANTUM Design Model MPMS instrument. $Hg[Co(NCS)_4]$ was used as a calibrant (susceptibility at 20 °C, 16.44×10^{-6} $cm^3\ mol^{-1}$). The molar susceptibilities were corrected for diamagnetism using Pascal's constants. Corrections were estimated at -241.90×10^{-6}, -202.24×10^{-6} and -201.58×10^{-6} $cm^3\ mol^{-1}$ for all the atoms of **3**, **4** and **5**, respectively. The electrochemical cell (10 cm^3) was a conventional one with three electrodes: working electrodes, Platinum Pt (diameter 2 mm, EDI Tacussel) for rotating disk electrode experiments (LSV, linear sweep voltammetry), Pt (disk diameter: 0.5 mm and 50 μm) for cyclic voltammetry experiments (CV), different disk ultramicroelectrodes (Pt 10 μm Tacussel, glassy carbon 10 μm PAR, gold 25 μm) for steady state experiments; counter electrode, Pt wire; and reference electrode, double junction SCE. The potential of ferricinium ion/ferrocene couple is 0.486 V vs. this [23] or 0.400 V vs. the standard hydrogen electrode SHE [24]. The experiments were carried out in dmf/Bu_4NPF_6 0.2 M under argon atmosphere; dmf (Acros, spectrosol) and Bu_4NPF_6 (Fluka, electrochemical grade) were used without further purification. The cyclic voltammetry was performed with the ohmic drop correction by positive feedback. The ohmic term R_u (uncompensated resistance) was first determinated by the current interrupt method [25]. The analysis of the cyclic voltammograms is helped by the use of simulation procedures (Nervi's program) [1].

2.2. Preparation of $Na_2(2,4\text{-}NCNsq)\cdot 2H_2O$; $Na_2L\cdot 2H_2O$ (**1**) and $(Ph_4P)_2L\cdot 4H_2O$ (**2**)

$Na_2L\cdot 2H_2O$ (**1**) was obtained by reaction of cyanamide with the 2,4-dimethylaminocyclobutene diolate according to a method adapted from Köhler et al. [5]. Cyanamide (0.336 g, 8 mmol) was added to a sodium ethoxide solution (Na 0.15 g, 6.5 mmol, EtOH 50 mL) and the mixture was stirred for 1 h; after this time the 2,4-dimethylaminocyclobutene diolate was added by portions. This new solution was heated under reflux for 5 h. At the beginning of the heating, the solution became rapidly yellow. A white-yellow powder was obtained and recrystallized from H_2O/EtOH (1/1) to give a pale yellow powder of analytically pure $Na_2L\cdot 2H_2O$ (**1**). Yield: 82%. *Anal*. Calc. for $C_6N_4Na_2O_2\cdot 2H_2O$: C, 29.75; H, 1.65; N, 23.14. Found: C, 29.53; H, 1.62; N, 22.88%. IR data (KBr disc) cm^{-1}: 3525m, 3306m, 3249m, 2304w, 2283w, 2180vs, 2163s, 1653m, 1564vs, 1541m, 1477vs (br), 1397vs (br), 1192w, 1132m, 936m, 789w, 703m (br), 629m, 572m, 537m. These values agree with those found by Köhler et al. [5].

$(Ph_4P)_2L\cdot 4H_2O$ (**2**) was prepared by mixing in a 2:1 ratio Ph_4PBr and $Na_2L\cdot 2H_2O$ in water. An orange yellow

[1] Simulated voltammograms (ESP) have been computed with Nervi's program. Copyright by Professor Carlo Nervi. This package can be downloaded at the Internet address: http://lem.ch.unito.it/chemistry/electrochemistry.html.

solid precipitated immediately. It was filtered off, washed with water and dried under vacuum. Yield: 99%. Yellow needle shape crystals of this compound were obtained after slow evaporation of the aqueous solution. *Anal.* Calc. for $C_{27}H_{24}N_2O_3P$: C, 71.20, H, 5.31; N, 6.15. Found: C, 71.25, H, 4.88, N, 6.34%. IR data (KBr disc) cm^{-1}: 3512w, 3429m (br), 3061m, 2126vs, 1631w, 1585m, 1562s, 1541m, 1482m, 1435vs, 1413vs, 1183w, 1163w, 1107vs, 1025w, 996m, 904w, 848w, 761m, 723s, 693m, 619w, 576w, 526vs, 503m, 461w.

2.3. Preparation of complexes 3, 4 and 5

2.3.1. $[Ni(Him)_4L \cdot 2H_2O]_n$ (3)

An aqueous solution (50 mL) of a mixture of $Na_2L \cdot 2H_2O$ (0.242 g, 1 mmol) and imidazole (Him) (1.36 g, 20 mmol) was added dropwise to a water solution (20 mL) of $Ni(NO_3)_2 \cdot 6H_2O$ (0.291 g, 1 mmol). The pale purple precipitate obtained was recrystallized in 100 mL of water. From slow evaporation of this solution, purple crystals of **3** were obtained. Yield: 28%. *Anal.* Calc. for $C_{18}H_{20}N_{12}O_4Ni$: C, 41.01; H, 3.82; N, 31.89. Found: C, 40.63; H, 3.23; N, 31.67%. IR data (KBr disc) cm^{-1}: 3406m, 3230m (br), 3126m, 2959w, 2861w, 2186vs, 2153s, 1577s (br), 1539s, 1430(sh), 1416vs (br), 1325m, 1256w, 1169w, 1125w, 1096w, 1070s, 939w, 919w, 865w (br), 833w, 751m, 665m, 617m, 593w, 573w, 560w.

2.3.2. $[Ni(Him)_3(H_2O)L \cdot H_2O]_n$ (4)

Green crystals of **4** co-crystallized with **3** during the slow evaporation of the previous solution. Yield: 34%. *Anal.* Calc. for $C_{15}H_{16}N_{10}O_4Ni$: C, 39.25; H, 3.51; N, 30.51. Found: C, 38.95; H, 3.25; N, 30.39. IR data (KBr disc) cm^{-1}: 3539w, 3410m (br), 3229m, 3124m, 2960w, 2854w, 2186s, 2137vs, 1632w, 1561s, 1536s, 1452vs (br), 1407vs, 1327m, 1255m, 1209w, 1174w, 1124w, 1105w, 1068s, 945w, 939w, 913w, 874w, 851w, 789w, 765w, 746m, 666m, 660m, 614m, 580w, 562w, 432w (br).

2.3.3. $[Ni(Him)_2(H_2O)_2L \cdot 3H_2O]_n$ (5)

An aqueous solution (100 mL) containing $Ni(NO_3)_2 \cdot 6H_2O$ (0.436 g, 1.5 mmol) and imidazole (0.204 g, 3 mmol) is added dropwise to a solution of 0.726 g of $Na_2L \cdot 2H_2O$ (3 mmol) in 100 mL of water. A blue precipitate was filtered off and recrystallization in water gave blue crystals of **5**. Yield: 32%. *Anal.* Calc. for $C_{12}H_{18}N_8O_7Ni$: C, 32.39; H, 4.08; N, 25.18. Found: C, 32.35; H, 3.75; N, 24.84%. IR data (KBr disc) cm^{-1}: 3425–3124m, 2967w, 2361w, 2202vs, 2157m (sh), 1787w, 1568m, 1538s, 1418vs (br), 1328m, 1208w, 1128w, 1097w, 1072m, 945w, 939w, 918w, 853w, 741w, 664w, 657m, 629w, 617w, 562w.

2.4. X-ray data collection and structure determinations

Data were collected at low temperature, respectively, at $T = 180$ K for **2**, **3** and **5**, and at $T = 160$ K for **4**. Compounds **2** and **4** were measured on a STOE one circle Imaging Plate Detector System CCD equipped with an Oxford Cryosystems Cryostream cooler device, and an Oxford Diffraction Kappa four circles system coupled with an Oxford Diffraction Cryojet cooler device was used for compounds **3** and **5**. For all compounds, a crystal decay was monitored and any fluctuations of the intensity were observed during data collection. Final unit cell parameters were obtained by the least-squares refinement of a set of well measured reflections. Structures were solved by direct methods using (SIR 92) [26] and refined by least-squares procedures on F^2 using SHELXL-97 [27]. All hydrogen atoms were located on the difference Fourier maps, but were introduced in calculation in idealized positions with an isotropic thermal parameter fixed, respectively, at 20% higher than those of the $C(sp^2)$ atoms to which they were connected. Excepted for hydrogen atoms of water molecules whose coordinates were fixed and U[iso] refined using a free variable, all non hydrogen atoms were anisotropically refined. Least-squares refinement were carried out by minimizing the function $\sum w(|F_o| - |F_c|)^2$, where F_o and F_c are the observed and calculated structure factors. A weighting scheme was used in the last refinement cycle, where weights are calculated from the following expression: $w = [\text{weight}]*[1 - (\Delta(F)/6*(F))]^2$. Models reached convergence with $R_1 = \sum \| F_o| - |F_c \| / \sum |F_o|$ and $wR_2 = [\sum w(F_o^2 - F_c^2)^2 / \sum w(F_o^2)^2]^{1/2}$, the criterion for a satisfactory complete analysis was the ratios of rms shift to standard deviation being less than 0.1 and no significant features in the final difference maps. All calculations were performed by using WINGX programs version 1.64 04 [28]. Drawings of molecules were realized with the aid of ORTEP32 [29], excepted for **5** for which the Cameron software [30] was used and the atomic scattering factors were taken from International tables for X-ray crystallography [31].

3. Results and discussion

The 2,4-NCNsq^{2-} (L^{2-}) dianion has been previously the subject of spectroscopic studies [5] but we have, for the first time, established its molecular structure as the ditetraphenylphosphonium salt. The first coordination complexes of this dianion have been obtained and characterized by single crystal X-ray diffraction: three distinct polymers can be isolated from the reaction of the L^{2-} dianion with nickel(II) in the presence of imidazole. $[Ni(Him)_4L \cdot 2H_2O]_n$ (**3**), and $[Ni(Him)_3(H_2O)L \cdot H_2O]_n$ (**4**) co-crystallized in a reaction mixture containing nickel(II)/$Na_2L \cdot 2H_2O$ (1:1) and a large excess of imidazole. $[Ni(Him)_2(H_2O)_2L \cdot 3H_2O]_n$ (**5**) was obtained from an aqueous solution containing 2 equiv. of $Na_2L \cdot 2H_2O$ and 2 equiv. of imidazole per nickel atom.

3.1. Crystal structures

Crystallographic data are summarized in Table 1.

Selected bond lengths and angles from the structural determinations of the salt **2** and of complexes **3**, **4** and **5**

Table 1
Crystallographic data for $(Ph_4P)_2L \cdot 4H_2O$ (**2**), $[Ni(Him)_4L \cdot 2H_2O]_n$ (**3**), $[Ni(Him)_3(H_2O)L \cdot H_2O]_n$ (**4**) and $[Ni(Him)_2(H_2O)_2L \cdot 3H_2O]_n$ (**5**)

	2	**3**	**4**	**5**
Formula	$C_{27}H_{24}N_2O_3P$	$C_9H_{10}N_6O_2Ni_{0.5}$	$C_{15}H_{16}N_{10}O_4Ni$	$C_{12}H_{18}N_8O_7Ni$
M	455.46	263.59	459.09	445.05
Crystal system, space group	triclinic, $P\bar{1}$	monoclinic, $P2_1/a$	triclinic, $P\bar{1}$	monoclinic, $P2_1/c$
a (Å)	9.1929(11)	8.1382(5)	8.7197(10)	8.0640(7)
b (Å)	10.6370(10)	15.2089(9)	10.7245(13)	14.8991(13)
c (Å)	12.0398(14)	9.5381(7)	11.2267(13)	16.1880(13)
α (°)	86.371(9)		82.742(14)	
β (°)	81.459(10)	93.494(5)	68.829(13)	99.777(7)
γ (°)	80.277(9)		73.240(14)	
U (Å^3)	1146.6(2)	1178.37(13)	937.12(19)	1916.7(3)
Z	4	4	2	4
D_c (g cm^{-3})	1.319	1.486	1.627	1.542
$F(000)$	478	544	472	920
θ Range (°)	3.42–26.37	3.43–33.54	2.60–24.41	3.02–26.37
T (K)	180 ± 2	180 ± 2	160 ± 2	180 ± 2
Number of measured reflections	8362	41 576	7486	13 766
Number of independent reflections	4644	4354	2865	3902
R_{int}	0.0325	0.0291	0.0314	0.0459
R_1[a] observed all	0.0464, 0.0669	0.0371, 0.0412	0.0245, 0.0265	0.0399, 0.0487
wR_2[b] observed, all	0.0949, 0.1039	0.0899, 0.0978	0.0634, 0.0644	0.1068, 0.1127

[a] $R_1 = \Sigma\|F_o| - |F_c\|/\Sigma|F_o|$.
[b] $wR_2 = [\sum w(F_o^2 - F_c^2)^2 / \sum w(F_o^2)^2]^{1/2}$.

are given in Tables 2–5, respectively. The structures of the three nickel(II) complexes will be compared to that obtained for the free 2,4-NCNsq^{2-} (L^{2-}) dianion in **2**.

3.1.1. Crystal structure of $(Ph_4P)_2L \cdot 4H_2O$ (2)

A view of the 2,4-NCNsq^{2-} (L^{2-}) dianion, along with the numbering scheme, is shown in Fig. 1. The L^{2-} ions are stacked along both the crystallographic a and c axes with interplanar distances of 9.193(5) and 12.040(5) Å, respectively. A stacking view of L^{2-} is presented in Fig. 2. The quasi-square planar ring is located around a crystallographic inversion centre. This plane includes the atoms directly attached to the ring O1 and N2. The C2–C3 and C2–C3′ distances (1.463(3) and 1.450(3) Å, respectively), are indicative of a π delocalized system. The C3–O1 distance (1.246(2) Å) is normal for a carbonyl group and is similar to those found in the 3,4-NCNsq^{2-} dianion [32] and in the 2,4-bis(dicyanomethylene)cyclobutane-1,3-dione dianion (2,4-dcmsq^{2-}) [6]. The NCN groups deviate from the ring plane by an angle of 20.6°. This structure is similar to those of the dicyd^{2-} derivatives because, excepted for the tetramethyl derivative [33], all these compounds are approximately planar with an anti conformation [34]. The three C–N distances in the sequence N(nitrile)–C–N(amido)–C(cycle) are 1.152(3), 1.351(3) and 1.325(3) Å, respectively, the first one being similar to the C–N(nitrile) distances observed in 2,4-dcmsq^{2-} (1.153(4) and 1.149(5) Å) [6]. Thus, the dianion is best represented as an extended π delocalized system.

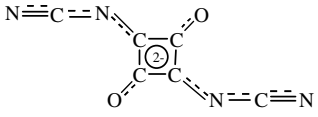

The hydrogen bond network involves the hydrogen atoms of two water molecules (O1w and O2w) and, as acceptors, the oxygen and nitrile nitrogen (N1) atoms of the ligand L^{2-} and O2w.

The distances and angles at the tetraphenylphosphonium ions are normal and are given as supplementary materials.

Table 2
Selected bond lengths (Å) and angles (°) for $(Ph_4P)_2L \cdot 4H_2O$ (**2**) with e.s.d.'s in parentheses

C1–N1	1.152(3)	C1–N2	1.351(3)	C2–N2	1.325(3)
C2–C3	1.463(3)	C2–C3′	1.450(3)	C3–O1	1.246(2)
N1–C1–N2	172.1(2)	C1–N2–C2	117.45(18)		
N2–C2–C3	130.5(2)	N2–C2–C3′	138.2(2)		
C3–C2–C3′	91.30(17)	C2–C3–C2′	88.70(17)		
C2–C3–O1	136.5 (2)	C2′–C3–O1	134.8(2)		

Symmetry operation: $-x, -y+1, -z+2$.

3.1.2. Crystal structures of complexes: $[Ni(Him)_4L \cdot 2H_2O]_n$ (3), $[Ni(Him)_3(H_2O)L \cdot H_2O]_n$ (4) and $[Ni(Him)_2(H_2O)_2L \cdot 3H_2O]_n$ (5)

The three complexes are polynuclear with, in each case, a bidentate 2,4-NCNsq^{2-} ligand bridging two nickel atoms through the nitrile functions and adopting an *anti* conformation. Views of the compounds **3**, **4** and **5** are shown in Figs. 3–5, respectively.

The structure of **3** is made of infinite chains of $[Ni(Him)_4L]$ units with two uncoordinated water molecules per unit cell. The nickel atom is located around a crystallographic inversion centre and a second inversion centre is

Table 3
Selected bond lengths (Å) and angles (°) for $[Ni(Him)_4L \cdot 2H_2O]_n$ (**3**) with e.s.d.'s in parentheses

Ni–N1	2.0946(11)	Ni–N3	2.0952(11)	Ni–N5	2.1018(11)
C1–N1	1.1548(17)	C1–N2	1.3217(16)	N2–C2	1.3274(17)
C2–C3	1.4599(18)	C2–C3′	1.4589(19)	C3–O1	1.2427(16)
N1–Ni–N1″	180.00(8)	N1–Ni–N3	90.58(4)	N1–Ni–N5	89.88(5)
N3–Ni–N5	91.93(4)	Ni–N1–C1	170.22(11)	N1–C1–N2	173.74(14)
C1–N2–C2	117.74(11)	N2–C2–C3	131.59(12)	N2–C2–C3′	137.84(12)
C2′–C3–C2	89.43(10)	C3′–C2–C3	90.57(10)	C2–C3–O1	135.31(13)
C2′–C3–O1	135.26(12)				

Symmetry operations: ′: $-x+1, -y, -z+1$, ″: $-x, -y, -z$.

Table 4
Selected bond lengths (Å) and angles (°) for $[Ni(Him)_3(H_2O)L \cdot H_2O]_n$ (**4**) with e.s.d.'s in parentheses

Ni–N1	2.1894(15)	Ni–N3	2.0731(15)	Ni–N5	2.0770(14)
Ni–N7	2.0621(15)	Ni–N9	2.0741(15)	Ni–O1w	2.1407(14)
C1–N1	1.164(2)	C1–N2	1.315(2)	C2–N2	1.323(2)
C4–N3	1.158(2)	C4–N4	1.308(2)	C5–N4	1.322(2)
C2–C3	1.454(2)	C2–C3′	1.460(2)	C5–C6	1.458(2)
C5–C6″	1.459(3)	C3–O1	1.248(2)	C6–O2	1.246(2)
N1–Ni–O1w	83.45(6)	N3–Ni–O1w	88.03(6)	N5–Ni–O1w	88.17(6)
N7–Ni–O1w	90.75(6)	N9–Ni–O1w	175.54(5)	N1–Ni–N3	85.38(6)
N1–Ni–N5	90.67(6)	N1–Ni–N7	172.38(6)	N1–Ni–N9	92.12(6)
N3–Ni–N5	174.80(6)	N3–Ni–N7	89.49(6)	N3–Ni–N9	91.09(6)
N5–Ni–N7	94.11(6)	N5–Ni–N9	92.43(6)	Ni–N1–C1	128.68(13)
Ni–N3–C4	173.77(14)	N1–C1–N2	173.45(19)	N3–C4–N4	172.47(18)
C1–N2–C2	117.34(14)	C4–N4–C5	118.56(15)	N2–C2–C3	131.90(15)
N2–C2–C3′	137.89(16)	C2–C3–C2′	89.79(14)	C3–C2–C3′	90.21(14)
C2–C3–O1	135.46(16)	C2′–C3–O1	134.75(16)		
N4–C5–C6	131.58(16)	N4–C5–C6″	137.53(16)	C5–C6–C5″	89.11(14)
C6–C5–C6″	90.89(14)	C5–C6–O2	136.34(16)	C5″–C6–O2	134.54(16)

Symmetry operations: ′: $-x+2, -y, -z$, ″: $-x+2, -y+1, -z$.

present in the middle of the squarate ring. The nickel atom is octahedrally bounded to four nitrogen atoms of four imidazole molecules and two nitrile nitrogen atoms of two 2,4-$NCNsq^{2-}$ ligands which are in *trans* positions. So, this complex may be compared with the monomer $[Ni(NO_2\text{-}NCN)_2(1\text{-meiz})_4]$ (where 1-meiz = 1-methylimidazole) that contains cyanamido ligands in *trans* positions [35]. In **3**, the Ni-ligand distance values go from 2.0946(11)

Table 5
Selected bond lengths (Å) and angles (°) for $[Ni(Him)_2(H_2O)_2L \cdot 3H_2O]_n$ (**5**) with e.s.d.'s in parentheses

Ni–N1	2.057(2)	Ni–N4	2.063(2)	Ni–N5	2.057(2)
Ni–N7	2.069(2)	Ni–O1w	2.1248(16)	Ni–O2w	2.1459(16)
C1–N1	1.149(3)	C1–N2	1.322(3)	C2–N2	1.332(3)
C6–N4	1.152(3)	C6–N3	1.315(3)	C4–N3	1.323(3)
C2–C3	1.447(3)	C3–C4′	1.454(3)	C4′–C5	1.465(3)
C2–C5	1.461(3)	C3–O1	1.252(3)	C5–O2	1.236(3)
C7–N5	1.322(3)	C7–N6	1.336(3)	C8–N6	1.366(4)
C9–N5	1.377(3)	C8–C9	1.358(4)		
C10–N7	1.307(3)	C10–N8	1.349(3)	C11–N8	1.362(4)
C12–N7	1.382(3)	C11–C12	1.351(4)		
N1–Ni–O1w	87.94(8)	N1–Ni–O2w	87.18(7)	N1–Ni–N5	93.24(8)
N1–Ni–N7	91.53(9)	N1–Ni–N4	172.03(9)	N4–Ni–O1w	86.41(7)
N4–Ni–O2w	86.71(7)	N4–Ni–N5	92.40(8)	N4–Ni–N7	93.74(8)
O1w–Ni–O2w	84.93(6)	O1w–Ni–N7	176.22(7)	O1w–Ni–N5	90.16(7)
O2w–Ni–N7	91.31(7)	O2w–Ni–N5	175.05(7)	N7–Ni–N5	93.61(8)
Ni–N1–C1	176.9(2)	N1–C1–N2	173.5(3)	C1–N2–C2	117.9(2)
Ni–N4–C6	167.5(2)	N4–C6–N3	173.3(3)	C6–N3–C4	117.4(2)
N2–C2–C3	131.5(2)	N2–C2–C5	137.4(2)	C3–C2–C5	91.04(18)
N3–C4–C3″	137.3(2)	N3–C4–C5″	132.1(2)	C3″–C4–C5″	90.64(18)
C2–C3–C4′	89.63(18)	C2–C3–O1	136.0(2)	O1–C3–C4′	134.3(2)
C2–C5–C4′	88.69(18)	C2–C5–O2	134.8(2)	O2–C5–C4′	136.5(2)

Symmetry operations: ′: $x-1, -y+1/2, z+1/2$, ″: $x+1, -y+1/2, z-1/2$.

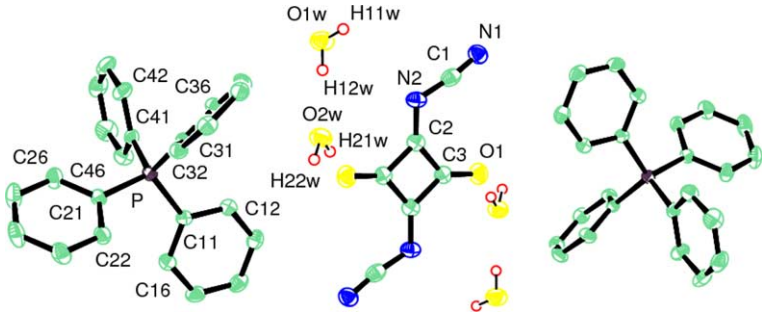

Fig. 1. ORTEP drawing of $(Ph_4P)_2L \cdot 4H_2O$ (**2**).

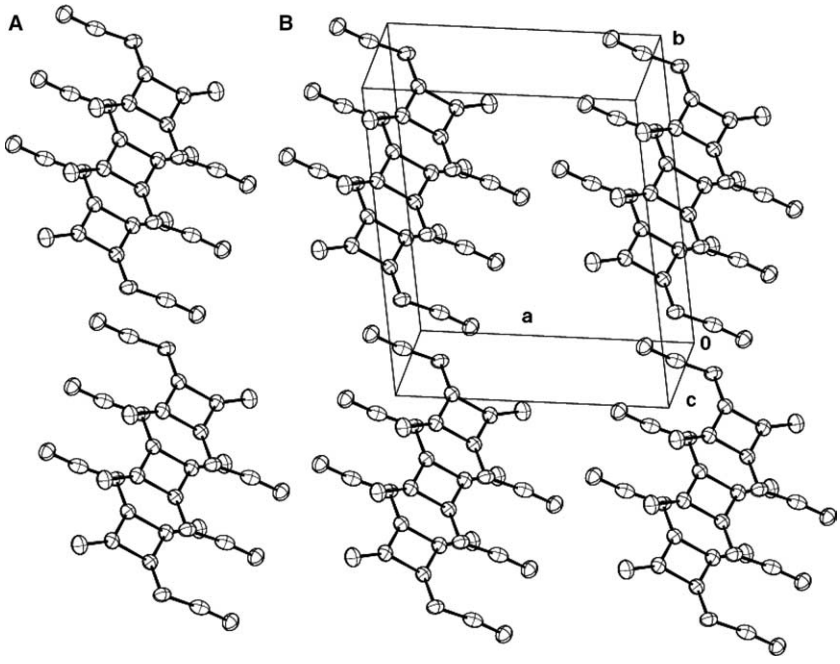

Fig. 2. View of a stacking (A) and side view of a columnar stacked structure (B) of $(Ph_4P)_2L \cdot 4H_2O$ (**2**).

to 2.1018(11) Å and angles around nickel are in the range 88.07(4)–91.93(4)°. It should be noted that the Ni-ligand distance values are in the same order of magnitude as those observed in the nickel complexes containing the 3,4-NCNsq^{2-} ligand (2.019(4)–2.151(2) Å) [9] or in the complex $[Ni(NO_2NCN)_2(1\text{-meiz})_4]$ where Ni–N = 2.100(3) Å

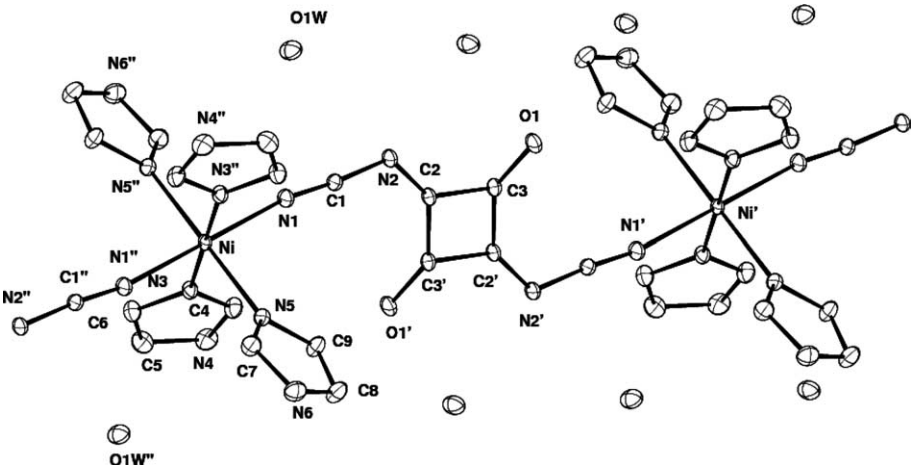

Fig. 3. ORTEP drawing of $[Ni(Him)_4L \cdot 2H_2O]_n$ (**3**).

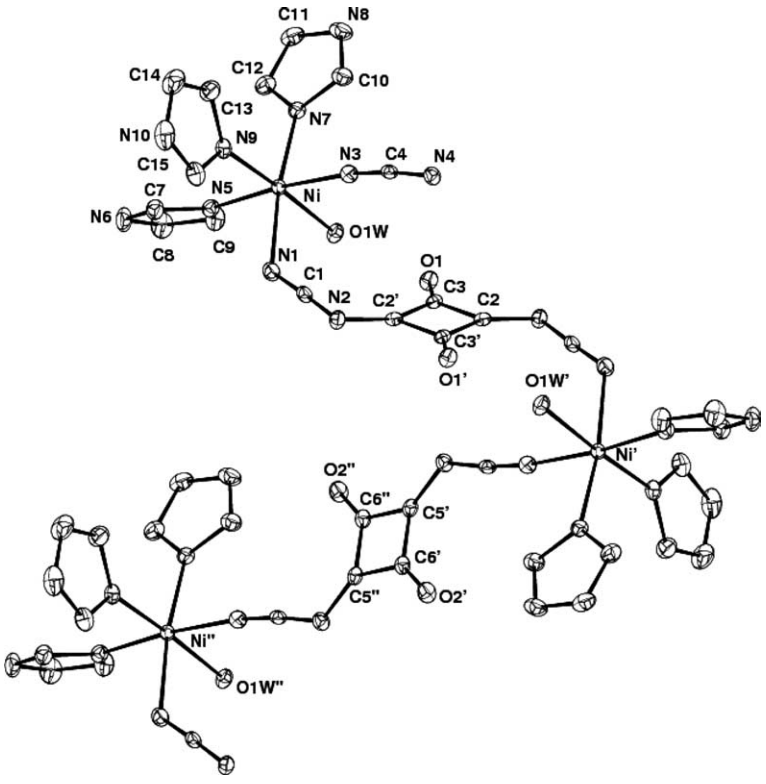

Fig. 4. ORTEP drawing of $[Ni(Him)_3(H_2O)L \cdot H_2O]_n$ (**4**).

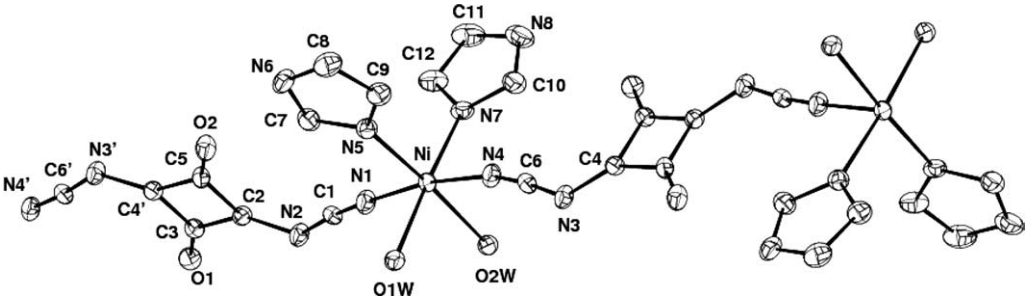

Fig. 5. ORTEP drawing of $[Ni(Him)_2(H_2O)_2L \cdot 3H_2O]_n$ (**5**).

[35]. However, the cyanamido coordination to the nickel atom can be stronger, as in [Ni(imd)(2-Clpcyd)] where $imd^- = 1.3$-bis-(2-pyridylimino)isoindolinato anion and 2-$Clpcyd^- = 2$-chlorophenylcyanamido anion (Ni–N = 1.874(10) Å) [36] or in $[Ni(NCN\text{-}2,6\text{-}Me_2C_6H_3)_2(PEt_3)_2]$ with Ni–N = 1.841(4) Å [37].

The C–C distance values in the squarate ring (1.4599(18) and 1.4589(19) Å) correspond to an aromatic system. The distances observed in the sequence N1(nitrile)–C1–N2(amido)–C2(cycle), 1.1548(17), 1.3217(16) and 1.3274(17) Å, respectively, are indicative of an extended π delocalized system and are not significantly modified by the coordination.

The Ni–C1–N1 angle of 170.22(11)° close to the 180° ideal value is characteristic of a nitrile end-on coordination of the cyanamido ligand. The squarate ring including the oxygen atoms is planar and the NCN groups deviate from the cycle plane by 6.66(0.15)°.

The shortest inter-chain Ni···Ni contact is 8.138(5) Å, while the intra-chain Ni···Ni distance is 12.155(5) Å.

The hydrogen bond network involves the hydrogen atoms of one of the two crystallisation water molecules of crystallisation (or hydration) (O1w) and the two nitrogen atoms of the imidazole molecules (N4 and N6) and, as acceptors, the oxygen and amido nitrogen (N2) atoms of the ligand L^{2-} and O1w.

The structure of **4** is made of infinite chains of $[Ni(Him)_3(H_2O)L]$ units with one uncoordinated water molecule per unit cell. The nickel atom environment is *cis* distorted octahedral, with three nitrogen atoms of three imidazole molecules, one oxygen atom of a water molecule and two nitrile nitrogen atoms of two 2,4-$NCNsq^{2-}$

ligands. The two largest Ni-ligand distance values are 2.1894(15) Å for Ni–N1 (N1 being the nitrile nitrogen atom of one 2,4-NCNsq^{2-} ligand) and 2.1407(14) Å for Ni–O1w while the other values vary from 2.0621(15) to 2.0770(14) Å. Moreover, compared with complex **3**, it should be noted that the substitution of one imidazole ligand by a water molecule induces a change in the coordination sphere of the nickel since the two squarate ligands are now in *cis* positions (N1–Ni–N3 angle of 85.38(6)°) and are, in this case, non equivalent. One cyanamido squarate is weakly coordinated to the metal atom (2.1894(15) Å for Ni–N1, the longest value observed for Ni–L distances in cyanamido squarate ligands, with a coordination angle Ni–N1–C1 of 128.68(13)°) and the other one is more strongly coordinated (2.0731(15) Å for Ni–N3 with a coordination angle Ni–N3–C4 of 173.77(14)°, quasi-linear nitrile coordination).

In this complex too, the C–C distance values in the two squarate rings correspond to aromatic systems (1.454(2)–1.460(2) Å). The deviations of the NCN groups from the cycle plane are 11.00° and 8.78°, respectively, for N1–C1–N2 and N3–C4–N4. The nitrile bonds are longer than in the free ligand: 1.164(2) Å for C1–N1 and 1.158(2) Å for C4–N3. The shortest distance between two delocalized systems is 8.720(5) Å.

The hydrogen bond network involves the hydrogen atoms of the two water molecules (O1w for the coordinated molecule and O2w for the molecule of crystallisation) and of three nitrogen atoms of imidazole molecules (N6, N8 and N10) and, as acceptors, the oxygen atoms and one nitrile nitrogen (N1) atom of the ligands L^{2-} and O2w.

The structure of **5** is made of infinite chains of $[Ni(Him)_2(H_2O)_2L]$ units with three uncoordinated water molecules per unit cell. With an even number of imidazole molecules, the two cyanamido squarate ligands are in *trans* positions, like in complex **3**. The geometry around the nickel atom is *cis* distorted octahedral with two water molecules weakly bonded in *cis* positions (2.1248(16) Å for Ni–O1w and 2.1459(16) Å for Ni–O2w), the other distances around the nickel atom range from 2.057(2) to 2.069(2) Å. The two Ni–L bond distances are similar (2.057(3) for Ni–N1 and 2.063(2) for Ni–N4′) with coordination angles of 176.9(2)° for Ni–N1–C1 and 167.5(2)° for Ni–N4′–C6′ which is close to the ideal value for nitrile coordination.

The C–C distances in the squarate ring, in the range 1.447(3)–1.465(3) Å, are indicative of a π delocalized system. Within the **3**–**5** series, the most perfect cyanamido squarate planarity is observed for complex **5**, since the deviation angles of the NCN groups from the squarate plane including the oxygen atoms are of 1.64° for N1C1N2 and of 1.23° for N4C6N3.

A stacking view of **5** along the *a* axis is presented in Fig. 6. The shortest distance between two delocalized systems is 8.063(5) Å.

The hydrogen bond network involves all the hydrogen atoms of the five water molecules and the two hydrogen atoms bonded to N6 and N8 in the imidazole molecules and, as acceptors, the oxygen atoms of the water molecules, the oxygen atoms and one amido atom N2 of the ligands L^{2-}.

3.2. IR spectroscopy

The IR spectra of cyanamides and related diimides have been already discussed [32,38–41]. It is now assumed that characteristic bands in the range 2200–2100 cm^{-1} are assigned to NCN asymmetrical stretching. We have previously observed that, in this area, the solid state spectra of 3,4-NCNsq^{2-} seem to largely depend on the nature of the counter ion. This is related to the prevalence of one of the two conformers A or B in the solid state. In solution, the two conformers coexist with the predominant form A.

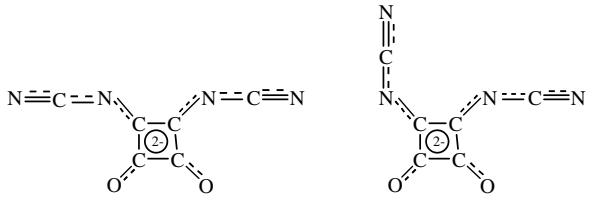

A — Tl^+ and PPh_4^+ salts — ν_a(NCN) = 2120 cm^{-1}

B — Na^+ salt — ν_a(NCN) = 2163 cm^{-1}

The same isomerism phenomenon is observed for the 2,4-NCNsq^{2-} salts. In the solid state, two conformers are observed: A in the PPh_4^+ salt **2** and B in the Na^+ salt **1** (ν_aNCN) = 2127 and 2180 cm^{-1}, respectively. In dmf solution, the two conformers coexist with the predominant form A (ν_aNCN) = 2126 cm^{-1} for **1** and **2**.

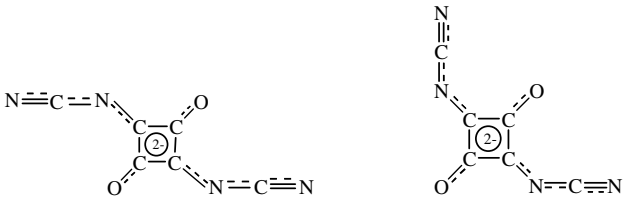

A — PPh_4^+ salt — ν_a(NCN) = 2127 cm^{-1}

B — Na^+ salt — ν_a(NCN) = 2180 cm^{-1}

Solid state IR data for the 2,4-NCNsq^{2-} salts **1** and **2** and for nickel complexes **3**–**5** are given in Table 6. In the three complexes, the cyanamido squarate ligands adopt the A conformation and are coordinated to the nickel atom by the nitrile groups, and, in each case, the (ν_aNCN) area of spectra is affected by complexation. The 2127 cm^{-1} value (ν_aNCN) of the free 2,4-NCNsq^{2-} in A conformation has been chosen as reference and compared with the solid

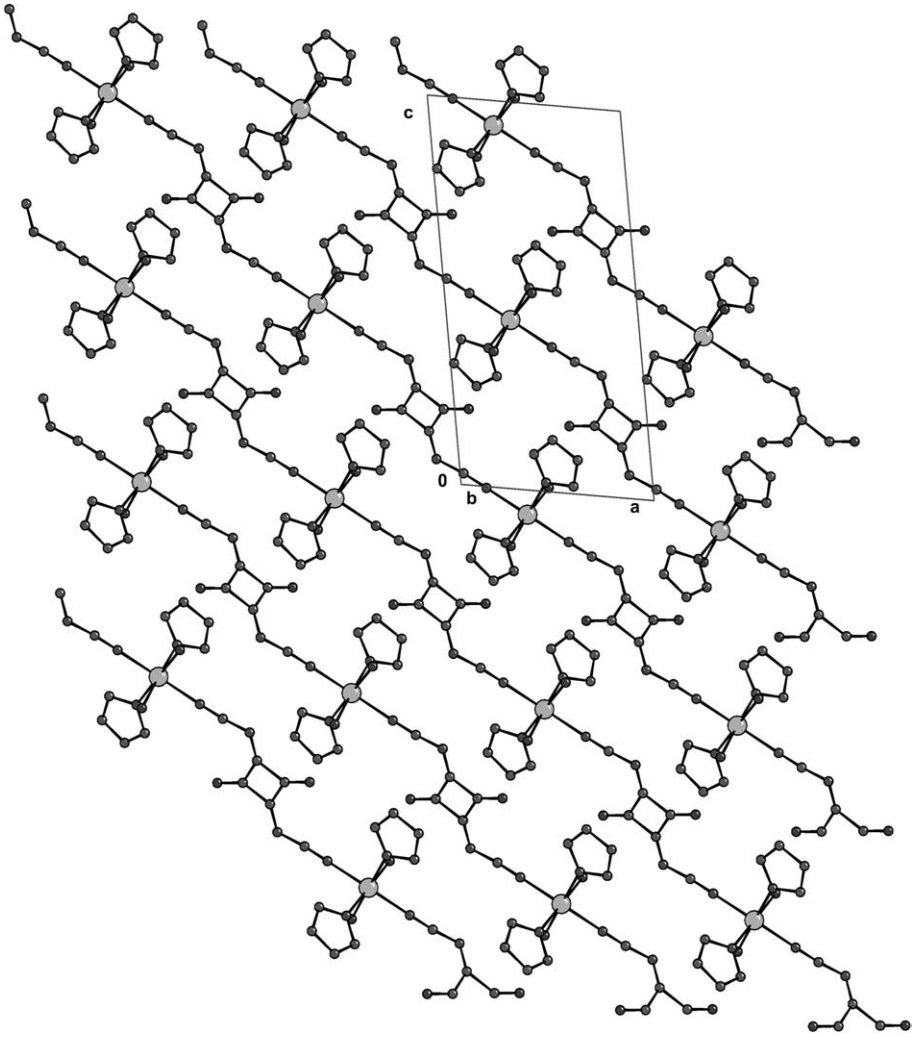

Fig. 6. View of a stacking of $[Ni(Him)_2(H_2O)_2L \cdot 3H_2O]_n$ (**5**).

Table 6
IR data for X_2(2,4-NCNsq) salts (X = Na **1**, PPh_4 **2**) and for complexes **3**, **4** and **5** (in cm^{-1}, in KBr pellets)

Compound	L^{2-} conformer	(ν_aNCN)	ν_{CO}	$\nu_{CO} + \nu_{CC}$	(ν_sNCN)
1	B	2180		1653–1477	1192; 1132
2	A	2127		1631–1413	1183; 1163
3	A	2186; 2153		1577–1416	1196; 1169
4	A	2186; 2137		1678–1407	1209; 1174
5	A	2202; 2157	1787	1568–1418	1208; 1128

state IR data of the complexes. The IR spectra of the three complexes showed two strong (ν_aNCN) bands and a positive average variation $\Delta\nu_{av}$ upon complexation is observed: +42 cm^{-1} in **3**, +34 cm^{-1} in **4**, +52 cm^{-1} in **5**.

In the spectra for **1**–**4**, one may notice the absence of the carbonyl stretching vibration between 1700 and 1800 cm^{-1} previously observed in derivatives of 3,4-$NCNsq^{2-}$ [8–10]. This may be attributed to the presence of an inversion centre in the middle of the squarate ring in compounds **1**–**4**. In complex **5**, where this inversion centre is lacking, a weak intensity band is observed at 1787 cm^{-1}. The infrared spectra of salts **1** and **2** and complexes **3**, **4** and **5** have in common a very strong and broad absorption centred at ca. 1500 cm^{-1} assigned to a combination of squarate C–O and C–C bond stretching vibrations. It should be noted that the weak bands assigned to (ν_sNCN) vibrations are observed in the range 1200–1130 cm^{-1}.

3.3. Magnetic data

The μ_{Ni} vs. temperature data for complexes **3**, **4** and **5** are shown in Fig. 7a.

The magnetic moments at 300 K were found to be 3.34 μ_B for **3**, 3.25 μ_B for **4** and 3.46 μ_B for **5**, slightly higher than the spin only value (2.83 μ_B) as usually observed for octahedral Ni(II) due to the second order spin–orbit coupling [42]. The temperature data are described by a Curie–Weiss law, yielding $C = 1.40\ cm^3\ K\ mol^{-1}$, $\theta = -9.89$ K for **3**, $C = 1.33\ cm^3\ K\ mol^{-1}$, $\theta = -7.12$ K for **4**, and $C = 1.50\ cm^3\ K\ mol^{-1}$, $\theta = -8.34$ K for **5**. For these polymeric complexes, the variation of the effective magnetic

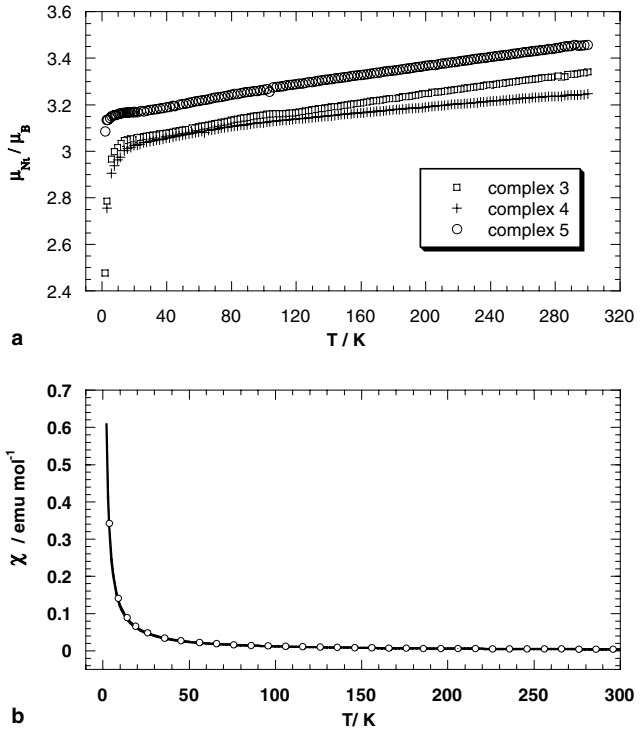

Fig. 7. (a) Temperature dependence of the effective magnetic moment for complexes **3** (□), **4** (+) and **5** (○). (b) Temperature dependence of the molar magnetic susceptibility for complex **5**. (○) experimental points; (—) calculated values.

moment within the 2–300 K domain agrees with that expected for essentially non-interacting nickel(II) ion with zero-field splitting effects [43].

The experimental magnetic susceptibility versus temperature curves have been obtained and the zero-field splitting equation [44] did not give satisfactory fittings.

The temperature dependence of the magnetic susceptibility of infinite isotropic Heisenberg chains, in the case $S = 1$, may be fitted by the following analytical expression (Eq. (1)) [45] which is only valid for an antiferromagnetic coupling ($J < 0$):

$$\chi_{\text{chain}} = (N\beta^2 g^2/\text{kT})[(2 + 0.0194X + 0.777X^2) /(3 + 4.346X + 3.232X^2 + 5.834X^3)] \quad (1)$$

with $X = |J|/\text{kT}$. The fitting of the experimental data with Eq. (1) led to the g_{Ni} and J (cm^{-1}) values: (2.26, −0.48), (2.20, −0.40) and (2.20, −0.05) for **3**, **4** and **5**, respectively. One example of the experimental and calculated (with Eq. (1)) magnetic susceptibilities versus temperature is shown in Fig. 7b (complex **5**). A similar behaviour is observed for complexes **3** and **4**.

This indicates that almost no coupling occurs between the nickel(II) atoms in complexes **3**–**5**, in agreement with the X-ray structural data giving 8.138 Å for the Ni···Ni shortest distances in **3**, 7.010 Å in **4**, and 7.686 Å in **5**. However, it may be noted that strong exchange coupling interactions at long distance are predicted with very similar ligands as dicyanamidobenzene-type molecules [46].

3.4. Solution studies

According to conductimetric measurements, the complexes are present in solution as neutral entities meaning that the 2,4-NCNsq^{2-} dianion is still coordinated to the nickel atom.

3.4.1. Electronic spectroscopy

Electronic spectra of complexes **3**, **4** and **5** in dmf solutions are dominated by the large π–π^* transition band of the ligand unchanged by complexation: 364 nm ($\log\varepsilon = 4.73$) for **1** and **2**, 364 nm ($\log\varepsilon = 4.46$) for **3**, 362 nm ($\log\varepsilon = 4.73$) for **4**, 362 nm ($\log\varepsilon = 4.71$) for **5**. In addition, weak energy d–d absorption bands, which values are consistent with a pseudo-octahedral environment of nickel(II) atom, have been observed: 1428 nm for **3**, 1386 and 640 nm for **4**, 1372 and 639 nm for **5**, with ε values lower than 70 L mol^{-1} cm^{-1}. They are assigned in increasing energy order to the transitions $^3T_{2g} \leftarrow {}^3A_{2g}$, $^3T_{1g}(F) \leftarrow {}^3A_{2g}$ and $^3T_{1g}(P) \leftarrow {}^3A_{2g}$. In the three complexes **3**–**5**, the bands corresponding to the third transition have not been clearly observed, as well as the one corresponding to the second transition for complex **3**.

3.4.2. Electrochemistry

In the electroactivity domain of dmf/Bu_4NPF_6, the cyclic voltammograms of the complexes present the same shape (Figs. 8, 9 and Table 7) and are compared to those of the free ligand L^{2-}. As already mentioned, the voltammogram of the free ligand shows two successive one-electron oxidations [47]:

The first step corresponds to the oxidation of the dianion into the radical-anion ($E_{1/2} = 0.40$ V),

$$L^{2-} \rightleftharpoons L^{-\bullet} + e^- \quad \text{system 1}$$

The second step corresponds to the oxidation of the radical-anion into the neutral form ($E_{1/2} = 1.10$ V),

$$L^{-\bullet} \rightleftharpoons L + e^- \quad \text{system 2.}$$

Moreover, an irreversible reduction process is observed which yields a *tetra*-anion by comparison of the oxidation and reduction peak currents ($E_p = -1.77$ V for a potential scan speed $v = 0.1$ V s^{-1}). This irreversible process is still present in the voltammograms of the complexes but badly defined. No evidence of Ni^{2+} reduction is given. The study has been restricted to the oxidation phenomena.

The electrooxidation of the ligand is more or less reversible as for its analogue 3,4-NCNsq^{2-} [9,41]. The voltammograms show the two redox systems 1 and 2 which are complicated by chemical reactions. As concerns the system 2, it appears that the ratio of the oxidation peak currents Ip_2/Ip_1 is always higher than 1 but decreases when the potential scan speed is enhanced and this system does not look like a reversible process. Taking into account the first one-electron process, system 2 consists in a one-electron transfer followed by a chemical reaction (opening of the ring, cyanamido function

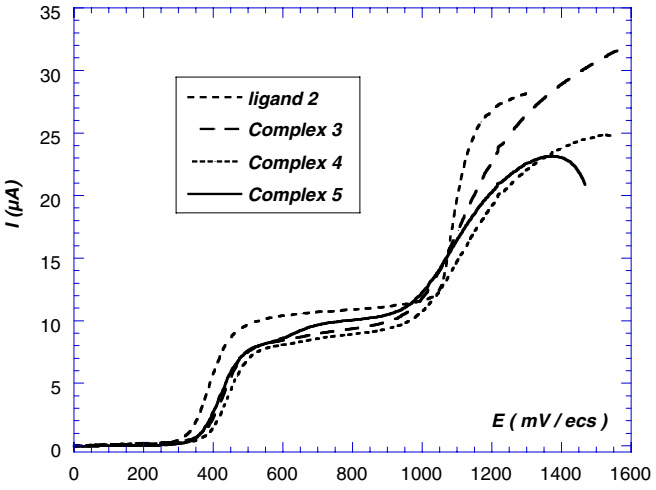

Fig. 8. Voltammograms at a rotating Pt disk electrode (diameter 2 mm) in dmf-Bu_4NPF_6 0.1 M, electrode rotation speed 1000 r.p.m., concentration 1 mM versus ligand **2** (reference electrode: double junction SCE): (- - -) L^{2-}, ligand **2**; (– –) complex **3**; (---) complex **4**; (—) complex **5**.

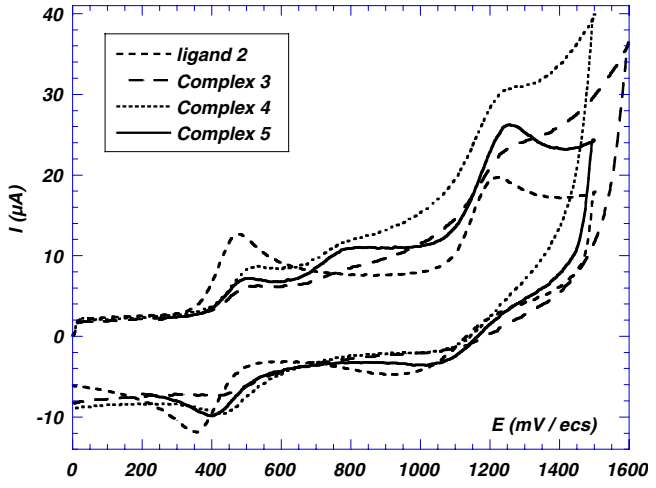

Fig. 9. Cyclic voltammograms at a Pt disk electrode (diameter 0.5 mm) in dmf-Bu_4NPF_6 0.1 M, potential scan speed 100 V s^{-1} (potential scanning starting at 0 V towards anodic potential and back to 0 V), concentration 1 mM versus ligand **2** (reference electrode: double junction SCE): (- - -) L^{2-}, ligand **2**; (– –) complex **3**; (---) complex **4**; (—) complex **5**.

Table 7
Cyclic voltammetry characteristics in dmf/Bu_4NPF_6: oxidation peak potential (V/ecs) at a potential scan speed 100 V s^{-1}, concentration 1 mM versus ligand 2

	L^{2-}, ligand **2**	Complex **3**	Complex **4**	Complex **5**
Couple $L^{\cdot-}/L^{2-}$	0.47	0.51	0.50	0.50
Couple $NiL^{\cdot+}/NiL$	–	0.80	0.78	0.80
Couple $L/L^{\cdot-}$	1.22	1.29	1.25	1.26

breaking or loss of π delocalization) and a further electrooxidation which explains the ratio Ip_2/Ip_1 higher than one. At a potential scan speed of 200 V s^{-1}, this chemical reaction is frozen and the voltammograms present the shape of a simple EE mechanism in which the first step is rapid and the second step is slower with a dissymmetric transfer coefficient around 0.3 [9].

The voltammograms of the complexes (Figs. 8, 9 and Table 7) are different from the ones of the free ligand. The first electron transfer (system 1) is split into two processes: by cyclic voltammetry, two oxidation peaks are observed ($E_p \approx 0.5$ and 0.8 V) and under hydrodynamic conditions, two waves replace the oxidation wave of system 1, especially for complex **5** (Fig. 8). Around 1.2 V, the oxidation process (system 2) is still present for the complexes, a slight displacement of the peak potentials is observed (Fig. 9) with an increase of the peak width. At a rotating electrode, electrode fouling is noticeable when the potential reaches the second plateau (system 2 – Fig. 8) and is enhanced when the rotation speed is increased.

When the potential scan speed is increased, the first peak ($E_p \approx 0.5$ V) decreases while the second ($E_p \approx 0.8$ V) increases readily; the peak corresponding to system 2 is little affected. Under stationary conditions (Fig. 8), a first look at the [0–1 V] region shows that the sum of the limiting currents for the complexes is lower than the limiting current of the free ligand. Assuming a total exchange of one electron for the first two steps, it appears that the diffusion coefficients are lower but in the same order of magnitude than the one of the free ligand. Furthermore, taking into account the null conductivity of the complexes solutions, this is consistent with the dissociation of the polymeric complexes into neutral monomers, which are the stable forms in solution. The number of Him ligands affects slightly the diffusion coefficients: complex **5** (2 Him ligands per nickel) presents the higher diffusion coefficient.

The electrochemical behaviour of these complexes is similar to that observed with Ni complexes of the 3,4-$NCNsq^{2-}$ dianion [9]. This phenomenon was explained by a square mechanism, representing the complexes by NiL where L^{2-} is the 2,4-$NCNsq^{2-}$ dianion:

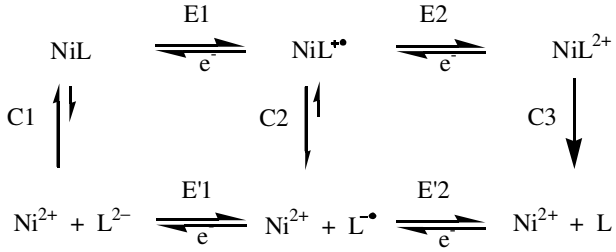

The electrochemical oxidation of the complexes follows two pathways which depend on the time scale of the experiment: E1–C2–E′2 represents the direct oxidation of the complex while C1–E′1–E′2 concerns the oxidation of the free ligand resulting from the chemical reaction C1. Using low potential scan speed, the main pathway is C1–E′1–E′2. When the potential scan speed is increased, reaction C1 is frozen and the pathway E1–C2–E′2 is observed. Whatever the potential scan speed is, no backward peak has been observed for E1 transfer (Fig. 9): reaction C2 is very fast.

The oxidized form $NiL^{+\cdot}$ is unstable because the unpaired electron would be localized on the NCN moiety [41] which is the coordinating arm in these complexes. This redox change modifies the coordinating ability of the NCN. This was not the case in copper or cobalt complexes with croconate violet in which coordination involves the oxygen atoms [48,49]. The radical anion of croconate violet presents an unpaired electron more or less localized on the dicyanomethylene groups and is still coordinated to the metal by the oxygen atoms.

The occurrence of the chemical reaction C1 is unexpected because conductimetric measurements showed that the NiL unit is not dissociated in dmf. Moreover, the anodic potential displacement of E′1–E1 (system 1, oxidation of L^{2-} into $L^{-\cdot}$ in the free form or coordinated one) is in agreement with the effect of an high complexation of the 2,4-$NCNsq^{2-}$ dianion but also with a poor complexation of the radical anion [50]. Considering the voltammograms, it appears that the dissociation C1 is related to the number of Him ligand. In Fig. 8, the E1 wave is well defined for complex **2**; in Fig. 9, the ratio $Ip(E1)/Ip(E'1)$ is also the highest one. This implies that the kinetic constant of the dissociation increases with the number of Him in the coordination sphere of the nickel ion.

Because of electrode fouling occurring on the second oxidation, it is difficult to analyse the behaviour of the complexes. At the potential scan speed used, no backward peak was found for the reverse E1 electron transfer which means that the occurrence of E2 electron transfer is uncertain; the second electron transfer would follow the E′2 pathway. However that may be, the radical complexes $NiL^{+\cdot}$ are unstable and cannot be isolated in order to study magnetic interactions. Nevertheless, according to the results of this study, the 2,4-$NCNsq^{2-}$ dianion appears to be an electrochemically switchable ligand [51].

4. Conclusion

In our previous works [8–10], we have studied the conformations of the 3,4-$NCNsq^{2-}$ ligand: two conformers (C_{2v} and C_s symmetries) have been structurally evidenced in complexes. In this work, concerning the 2,4-$NCNsq^{2-}$ dianion, the same conformer A (C_{2h} symmetry) is always observed in the molecular structures of the three nickel(II) polymers.

In the course of our studies, we have observed the diversity of the coordination modes obtained for these two ligands in ten complexes. This analysis reveals that the structures can be classified in two different types: those containing the amido coordination in the case of a copper(II) monomer [8] or a palladium dimer [10] and those containing the nitrile (end-on) coordination in a nickel(II) monomer [9], a copper(I) dimer [8], a copper(II) polymer [8] and five nickel(II) polymers [9, this work]. It appears that even if the end-on coordination often comes across in complexes of these cyanamido squarate ligands, they may be considered as multidentate ligands.

5. Supplementary material

Further details on the Crystal Structure Investigation are available on request from the Director of the Cambridge Crystallographic Data Centre, 12 Union Road, GB-Cambridge CB2 1EZ UK, on quoting the full journal citation (CCDC 257733-257736).

References

[1] R. West, D.L. Powell, J. Am. Chem. Soc. 85 (1963) 2577.
[2] H.E. Sprenger, W. Ziegenbein, Angew Chem., Int. Ed. Engl. 6 (1967) 553, and 7 (1968) 530.
[3] A.J. Fatiadi, Oxocarbons, Academic Press, New York, 1980.
[4] B. Gerecht, T. Kämpchen, K. Köhler, W. Massa, G. Offermann, R.E. Schmidt, G. Seitz, R. Sutrisno, Chem. Ber. 117 (1984) 2714.
[5] K. Köhler, W. Massa, G. Offermann, G. Seitz, R. Sutrisno, Chem. Ber. 118 (1985) 1903.
[6] P.-L. Fabre, C. Pena, A.M. Galibert, B. Soula, G. Bernardinelli, B. Donnadieu, P. Castan, Can. J. Chem. 78 (2000) 280.
[7] A.M. Galibert, B. Soula, B. Donnadieu, P.-L. Fabre, Inorg. Chim. Acta 313 (2001) 160.
[8] P.-L. Fabre, A.M. Galibert, B. Soula, F. Dahan, P. Castan, J. Chem. Soc., Dalton Trans. (2001) 1529.
[9] A.M. Galibert, O. Cortadellas, B. Soula, B. Donnadieu, P.-L. Fabre, J. Chem. Soc., Dalton Trans. (2002) 3743.
[10] O. Cortadellas, A.M. Galibert, B. Soula, B. Donnadieu, P.-L. Fabre, Inorg. Chim. Acta 357 (2004) 746.
[11] K. Yamada, M. Mizumo, Y. Hirata, Bull. Chem. Soc. Jpn. 31 (1958) 543.
[12] C.E. Xanthopoulos, M.P. Sigalas, G.A. Katsoulos, C.A. Tsipis, C.C. Hadjikostas, A. Terzis, M. Mentzafos, Inorg. Chem. 32 (1993) 3743.
[13] A. Aumüller, P. Erk, G. Klebe, S. Hünig, J.U. von Schütz, H.P. Werner, Angew. Chem., Int. Ed. Engl. 25 (1986) 740.
[14] A. Kobayashi, R. Kato, H. Kobayashi, T. Mori, H. Inokuchi, Solid State Commun. 64 (1987) 45.
[15] S. Hünig, A. Aumüller, P. Erk, H. Meixner, J.U. von Schütz, H.-J. Gross, U. Langohr, H.-P. Werner, H.C. Wolf, Ch. Burschka, G. Klebe, K. Peters, H.G. v Schnering, Synth. Met. 27 (1988) B181.
[16] H. Kobayashi, R. Kato, A. Kobayashi, T. Mori, H. Inokuchi, Solid State Commun. 65 (1988) 1351.
[17] A. Kobayashi, T. Mori, H. Inokuchi, R. Kato, H. Kobayashi, Synth. Met. 27 (1988) B275.
[18] S. Hünig, P. Erk, Adv. Mater. 3 (1991) 225.
[19] R.J. Crutchley, Coord. Chem. Rev. 219–221 (2001) 125, and references therein.
[20] (a) A. Escuer, N. Sanz, F.A. Mautner, R. Vicente, Eur. J. Inorg. Chem. (2004) 309, and references therein;
(b) M.A.S. Aquino, F.L. Lee, E.J. Gabe, C. Bensimon, J.E. Greedan, R.J. Crutchley, J. Am. Chem. Soc. 114 (1992) 5130;
(c) B.C. Gerstein, M. Habenschuss, J. Appl. Phys. 43 (1972) 5155.
[21] N.M. Rowley, R.J. Mortimer, Sci. Prog. 85 (2002) 243, and references therein.
[22] E.W. Neuse, B.R. Green, J. Org. Chem. 39 (1974) 3881.
[23] D. Ranchet, J.-B. Tommasino, O. Vittori, P.-L. Fabre, J. Sol. Chem. 27 (1998) 979.
[24] A.M. Bond, E.A. McLennan, R.S. Stojanovic, F.G. Thomas, Anal. Chem. 59 (1987) 2853.
[25] P. Cassoux, R. Dartiguepeyron, C. David, D. de Montauzon, J.-B. Tommasino, P.-L. Fabre, Actual. Chim. (1994) 49, and references therein.
[26] SIR-92, Program for Automatic Solution of Crystal Structures by Direct Methods A. Altomare, G.L. Cascarano, C. Giacovazzo, A. Guagliardi, M.C. Burla, G. Polidori, M. Camalli, J. Appl. Crystallogr. 27 (1994) 435.

[27] G.M. Sheldrick, SHELX-97 [Includes SHELXS 97, SHELXL 97, CIFTAB] – Programs for Crystal Structure Analysis (Release 97-2), Institüt für Anorganische Chemie der Universität, Tammanstrasse 4, D-3400 Göttingen, Germany, 1998.
[28] WINGX L.J. Farrugia, J. Appl. Crystallogr. 32 (1999) 837.
[29] ORTEP3 for Windows L.J. Farrugia, J. Appl. Crystallogr. 30 (1997) 565.
[30] CAMERON – A Molecular Graphics Package D.M. Watkin, L. Pearce, C.K. Prout, Chemical Crystallography Laboratory, University of Oxford, Oxford, 1993.
[31] D.T. Cromer, J.T. WaberInternational Tables for X-ray Crystallography, vol. IV, Kynoch Press, Birmingham, England, 1974.
[32] B. Lunelli, M. Monari, Z. Naturforsh. 44b (1989) 169.
[33] M.A.S. Aquino, F.L. Lee, E.J. Gabe, J.E. Greedan, R.J. Crutchley, Inorg. Chem. 30 (1991) 3234.
[34] M.A.S. Aquino, R.J. Crutchley, F.L. Lee, E.J. Gabe, C. Bensimon, Acta Crystallogr. C 49 (1993) 1543.
[35] M. Hvastijová, J. Kohout, J. Kožíšek, L. Jäger, J. García Díaz, Polyhedron 19 (2000) 1021.
[36] R.J. Letcher, W. Zhang, C. Bensimon, R.J. Crutchley, Inorg. Chim. Acta 210 (1993) 183.
[37] Y.-J. Kim, Y.-S. Joo, J.-T. Han, W.S. Han, S.W. Lee, J. Chem. Soc., Dalton Trans. (2002) 3611.
[38] H.G. Khorana, Chem. Rev. 53 (1953) 145.
[39] F. Kurzer, K. Douragui-Zadeh, Chem. Rev. 67 (1967) 107.
[40] R.J. Crutchley, M.L. Naklicki, Inorg. Chem. 28 (1989) 1955.
[41] B. Lunelli, S. Roffia, C. Paradisi, G.F. Pedulli, J. Chem. Soc., Faraday Trans. 90 (1994) 137.
[42] F.E. Mabbs, D.J. Machin, in: Magnetism and Transition Metal Complexes, Chapman and Hall Ltd., London, 1973.
[43] S.R. Batten, B.F. Hosskins, B. Moubaraki, K.S. Murray, R. Robson, J. Chem. Soc., Dalton Trans. (1999) 2977.
[44] (a) O. Kahn, in: Molecular Magnetism, VCH Publishers, Inc., New York, 1993 (Chapter 2);
(b) M.T. Azcondo, L. Ballester, A. Gutiérrez, M.F. Perpiñán, U. Amador, C. Ruiz-Valero, C. Bellitto, J. Chem. Soc., Dalton Trans. (1996) 3015.
[45] (a) A. Meyer, A. Gleizes, J.J. Girerd, M. Verdaguer, O. Kahn, Inorg. Chem. 21 (1982) 1729;
(b) L. Sacconi, F. Mani, A. Bencini, in: G. Wilkinson (Ed.), Comprehensive Coordination Chemistry, vol. 5, Pergamon Press, Oxford, 1987, p. 1.
[46] E. Ruiz, A. Rodriguez-Fortea, S. Alvarez, Inorg. Chem. 42 (2003) 4881.
[47] G. Seitz, P. Imming, Chem. Rev. 92 (1992) 1227.
[48] F. Dumestre, B. Soula, A.M. Galibert, P.-L. Fabre, G. Bernardinelli, B. Donnadieu, P. Castan, J. Chem. Soc., Dalton Trans. (1998) 4131.
[49] B. Soula, A.M. Galibert, B. Donnadieu, P.-L. Fabre, Inorg. Chim. Acta 90 (2001) 324.
[50] B. Trémillon, Electrochimie Analytique et Réactions en Solution, Masson, Paris, 1993 (Chapter X).
[51] A.E. Kaifer, M. Gómez-Kaifer, Supramolecular Electrochemistry, Wiley-VCH, Weinhem, 1999.